Nano Research
https://doi.org/10.1007/s12274-017-1792-z
Research Article
ISSN 1998-0124
CN 11-5974/O4

Tunable excitonic emission of monolayer WS_2 for the optical detection of DNA nucleobases

Shun Feng[1], Chunxiao Cong[2] (✉), Namphung Peimyoo[1,†], Yu Chen[1], Jingzhi Shang[1], Chenji Zou[1], Bingchen Cao[1], Lishu Wu[1], Jing Zhang[1], Mustafa Eginligil[3], Xingzhi Wang[1], Qihua Xiong[1], Arundithi Ananthanarayanan[4], Peng Chen[4], Baile Zhang[1], and Ting Yu[1] (✉)

[1] *Division of Physics and Applied Physics, School of Physical and Mathematical Sciences, Nanyang Technological University, Singapore 637371, Singapore*
[2] *School of Information Science and Technology, Fudan University, Shanghai 200433, China*
[3] *Key Laboratory of Flexible Electronics (KLOFE) & Institute of Advanced Materials (IAM), Jiangsu National Synergetic Innovation Center for Advanced Materials (SICAM), Nanjing Tech University (NanjingTech), 30 South Puzhu Road, Nanjing 211816, China*
[4] *Division of Bioengineering, School of Chemical and Biomedical Engineering, Nanyang Technological University, Singapore 637457, Singapore*
[†] *Present address: College of Engineering, Mathematics and Physical Sciences, University of Exeter, Exeter EX4 4QF, UK*

Received: 23 April 2017
Revised: 25 July 2017
Accepted: 6 August 2017

KEYWORDS
tungsten disulfide, photoluminescence, optical biosensing, chemical doping

ABSTRACT

Two-dimensional transition metal dichalcogenides (2D TMDs) possess a tunable excitonic light emission that is sensitive to external conditions such as electric field, strain, and chemical doping. In this work, we reveal the interactions between DNA nucleobases, i.e., adenine (A), guanine (G), cytosine (C), and thymine (T) and monolayer WS_2 by investigating the changes in the photoluminescence (PL) emissions of the monolayer WS_2 after coating with nucleobase solutions. We found that adenine and guanine exert a clear effect on the PL profile of the monolayer WS_2 and cause different PL evolution trends. In contrast, cytosine and thymine have little effect on the PL behavior. To obtain information on the interactions between the DNA bases and WS_2, a series of measurements were conducted on adenine-coated WS_2 monolayers, as a demonstration. The p-type doping of the WS_2 monolayers on the introduction of adenine is clearly shown by both the evolution of the PL spectra and the electrical transport response. Our findings open the door for the development of label-free optical sensing approaches in which the detection signals arise from the tunable excitonic emission of the TMD itself rather than the fluorescence signals of label molecules. This dopant-selective optical response to the DNA nucleobases fills the gaps in previously reported optical biosensing methods and indicates a potential new strategy for DNA sequencing.

Address correspondence to Chunxiao Cong, cxcong@fudan.edu.cn; Ting Yu, yuting@ntu.edu.sg

1 Introduction

Two-dimensional transition metal dichalcogenides (2D TMDs) have attracted increasing attention because of their extraordinary optical and electrical properties [1–3]. Unlike graphene, monolayer (1L) semiconductor TMDs, MX_2 (M = Mo, W; X = S, Se), possess a direct band gap that gives rise to an anomalously strong photoluminescence (PL) emission in the visible to near infrared range [4, 5]. The 2D confinement results in reduced dielectric screening and enhanced coulomb interactions, which further lead to relatively large binding energies of the electron–hole (e–h) quasiparticle-like neutral excitons (A), charged excitons or trions (A^-/A^+), and even biexcitons (AA) [6, 7]. These excitonic states are strongly correlated to the unique electronic structures of 2D semiconductors and are reflected by sharp and intense peaks in the PL spectra of these 2D semiconductors. Therefore, the energy and related emission states can be manipulated by tuning the electronic structure, such as by gate/chemical doping [8, 9], applying an external strain [10], or laser stimulation [11], and probed directly by optical and electrical measurements. Among these methods, the modulation of excitonic states via chemical approaches has become a promising research direction not only because of the efficient improvement in the optical qualities of 2D semiconductors on chemical treatment [12, 13] but also because the coupling between the chemical compounds and 2D materials indicates chemical sensing ability, arising from their large surface to volume ratios. Many efforts have been devoted to study the charge-transfer-induced interactions between 2D semiconducting TMDs and their surroundings including environmental molecules like H_2O and O_2 and typical dopants such as F4TCNQ [14, 15]. The investigation of the interactions of biomolecules with 2D semiconducting TMDs is still in its infancy, and most studies have been theoretical [16–18]. To date, experimental reports have focused on the fluorescent (FL) or chemiluminescent detection of DNA using liquid-phase exfoliated nanosheets of 2D semiconducting TMDs for optical sensing [19–22]. Specifically, the optical signals of these platforms originate from the fluorescence label molecules rather than the TMDs. In sharp contrast, the observation of tunable excitonic emissions directly from monolayer TMD samples upon the physisorption of biomolecules is rare, especially for the well-analyzed excitonic emission (A/A^-) features hidden in the spectra [23]. In this work, such changes in the PL spectra of 2D TMDs, which have been underestimated in previous biosensing studies, are monitored and shown to be useful biosensing indices. Compared to liquid-phase TMD samples in solution, solid-phase flakes on Si/SiO_2 wafer substrates are more suitable for developing sensing devices integrated on chips. For such applications, the exploration of the sensing abilities of chemical vapor deposited (CVD) TMDs is an essential step. Meanwhile, the CVD process could be used for mass production of these materials. Studies of the PL detection of biomolecules using CVD 2D semiconductor TMDs are scarce but crucial for the development of biosensing applications.

In recent years, researchers have made considerable efforts to use 2D materials as platforms for biological fluorescence sensing and imaging studies [24–26]. Among the various sensing targets, the development of a low-cost, convenient, label-free DNA detection platform has gained significant interest [27, 28]. Recently, several methods for the detection of specific DNA strands with TMDs based on Förster resonance energy transfer pairs have been reported [28]. However, these sensing tactics require complicated probe–target labeling processes, leaving the area of one-step optical detection relatively uninvestigated [19, 30]. Furthermore, previous studies have focused on larger molecules, such as particular DNA strands, while the detection of the nucleobases that form the strands has been ignored. Because the information within DNA is hidden inside the sequence of these bases, compared to the recognition of particular DNA strands, the detection of single bases could serve as an alternative pathway to decode many DNA molecules within one platform, leading to a possible solution to optical DNA sequencing [31]. In this regard, a one-step approach for the optical detection of nucleobases with 2D materials merits development. Note that semiconducting TMD materials stand out as candidates for this purpose because of their chemically tunable excitonic properties. To achieve such optical sensing applications, an investigation

of the impact of DNA bases on optical properties of semiconducting TMD material is useful.

In this work, the WS_2-nucleobase interaction is systematically studied. We performed PL spectroscopy measurements on CVD-grown monolayer WS_2 on a SiO_2/Si substrate both before and after coating with DNA nucleobase, i.e., adenine (A), guanine (G), cytosine (C), and thymine (T), solutions. We observed the conspicuous and distinguishable evolution of the excitonic states of the monolayer WS_2 upon the physisorption of adenine and guanine, whereas cytosine and thymine show a negligible influence, indicating the potential of CVD monolayer WS_2 for optically sensing DNA nucleobases. To reveal the sensing mechanism for DNA nucleobases and the doping of monolayer WS_2, the evolution of the PL profiles and the electrical transport features of monolayer-WS_2-based field effect transistors (FETs) were analyzed in detail. The results show that p-type doping is responsible for the optical effects. The typical doping level was further quantified by analyzing distinctive features in the PL spectra of monolayer WS_2 with various dopant concentration and calculated electron concentrations. These findings indicate the potential use of monolayer WS_2 for the optical detection of DNA nucleobases.

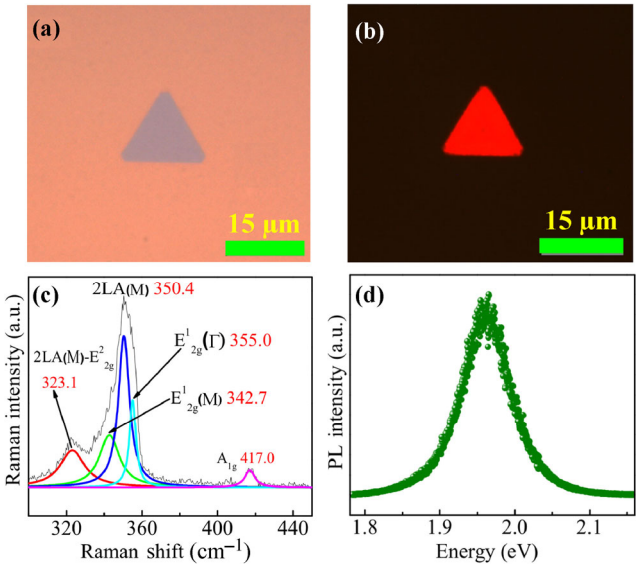

Figure 1 Characterization of WS_2 flakes. (a) Optical and (b) fluorescence images of CVD grown 1L WS_2 sample on SiO_2/Si substrate. (c) Lorentz-fitted Raman and (d) PL spectra of the WS_2 flakes at room temperature in air.

2 Results and discussion

Monolayer WS_2 flakes were chemically grown on a 300-nm SiO_2 layer capped on a highly doped Si wafer using CVD. We followed a method employed in previous studies on WS_2 growth [32, 33]. The prepared samples are symmetric and triangular with strong and homogeneous fluorescence emissions, as shown in Figs. S1(a) and S1(b) in the Electronic Supplementary Material (ESM). To further characterize the sample quality, both PL and Raman spectra were measured using a 2.33-eV (532-nm) continuous laser (only the A exciton was observed in the PL measurements). As shown in Fig. 1(c), the interpreted Raman features indicate that our sample is highly crystalline WS_2 containing phonon modes of in-plane vibrational E^1_{2g}(M) and E^1_{2g}(Γ) modes, the second-order longitudinal acoustic phonon 2LA(M), out-of-plane modes, and some combinational modes. A frequency difference of 62 cm^{-1} between the E^1_{2g}(Γ) and A_{1g} modes was observed. These signatures agree well with previous Raman studies of monolayer WS_2 [33–36]. Figure 1(d) shows the PL spectra of the as-prepared sample, where a distinct peak with an emission energy of 1.96 eV is observed. The peak position agrees well with the reported range of the A exciton emission of CVD-grown monolayer WS_2 at room temperature [32, 36]. By using Raman fingerprints and striking PL emissions, we confirmed that the monolayer WS_2 was obtained. The PL intensity of the as-grown CVD WS_2 is intrinsically higher than that of MoS_2 [32], even without any further chemical treatment [12, 13], making it more suitable for optical applications.

Concerning the shape of the PL spectrum, based on a previous study, it mainly contains peaks originating from two kinds of quasi-particles: neutral and charged excitons. Generally, if there are excessive electrons (holes) inside the sample, negative (positive) charged excitons could be formed [6]. Compared to the A, A^-/A^+ consist of an e–h pair with an additional electron or hole, resulting in different recombination behaviors and emission energies. Both states can be identified in the PL spectrum by peak fitting and assignment because of their different peak positions and peak widths. Therefore, the PL profile of WS_2 is sensitive

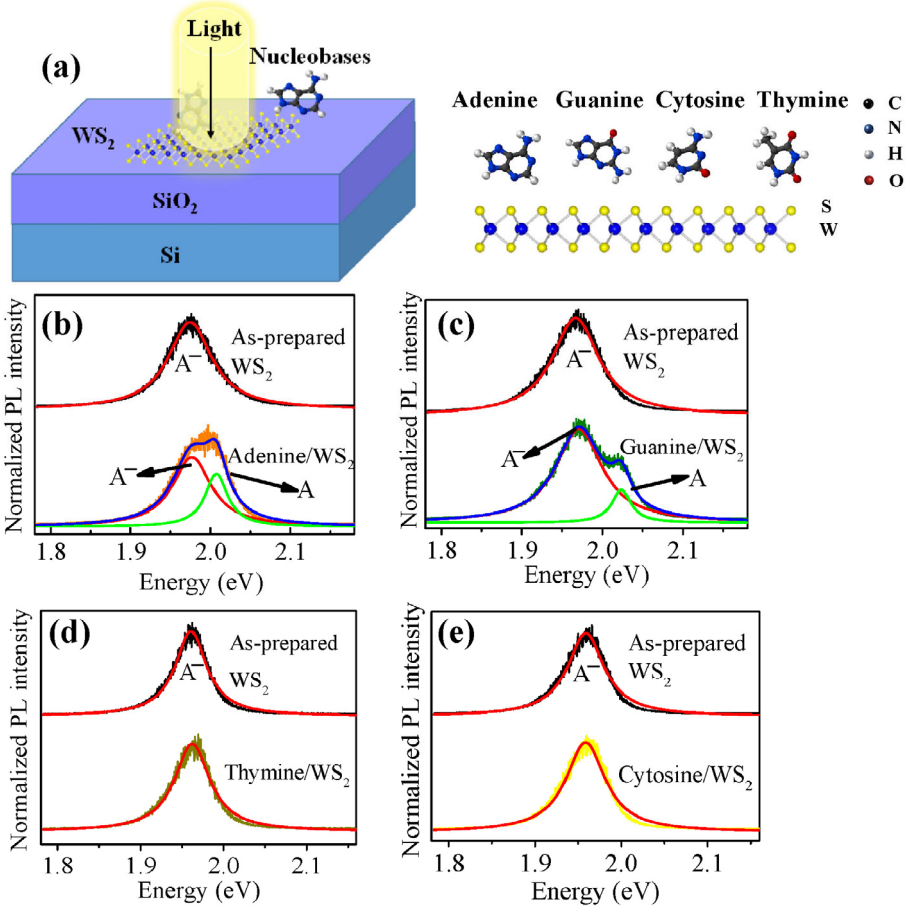

Figure 2 Optical detection of DNA nucleobases. (a) Schematic image of the optical nucleobase sensing platform, and (b)–(e) PL spectra of 1L WS_2 before and after being coated with 1 mM adenine, guanine, thymine, and cytosine solutions, respectively.

to the charge transfer induced by the adsorption of p/n-type dopant molecules.

As shown schematically in Fig. 2(a), the as-grown WS_2 on the SiO_2/Si wafer was spin coated with a DNA nucleobase solution and then exposed to laser light to record the PL spectra before and after the spin coating of the nucleobase solution, which makes it possible to study the effect of the nucleobases on WS_2 systematically. To validate that the optical responses arose from the nucleobases alone rather than solvent (ethanol), we conducted control experiments. The PL spectra (Fig. S1(a) in the ESM) recorded before and after the spin coating of pure ethanol on the sample contain identical features, which indicates that any further evolution is from the solute (i.e., nucleobases) rather than the solvent. In addition, this control experiment eliminates the potential interference of moisture doping from the ambient environment [8, 14].

The effects of four kinds of nucleobases on WS_2 were probed by PL measurements before and after coating with a 1 mM nucleobase solution, as shown in Figs. 2(b)–2(e). We found that adenine and guanine exhibit quantitatively different splitting effects on the PL profile (Figs. 2(b) and 2(c)), while cytosine and thymine (Figs. 2(d) and 2(e)) have a negligible impact on the PL features of WS_2. The different effects of the nucleobases on the PL features of WS_2 provide a convenient approach and rich possibilities for detecting and distinguishing the four bases.

The evolved PL features in Figs. 2(b)–2(e) can be further decomposed into multiple Lorentz peaks. Based on the fitted curves and referring to the literature [8], the lower energy peak can be identified as a negative trion, A^- (1.96 eV), whereas the higher energy peak originates from a neutral exciton, A (2.01 eV). In the spectra of WS_2, after coating with A/G bases, the neutral

exciton A peak emerges and dominates the PL spectra. A similar evolution is observed in the gate [7, 37] and chemically modulated [8, 14, 15] PL measurements. Based on these reports, this splitting signature is attributed to p-type doping. Because adenine gave rise to a more pronounced emerging neutral exciton peak compared to guanine, it is worth identifying the factors that dictate the magnitude of this optical evolution. Thus, we used adenine as an example to probe this PL splitting effect comprehensively and confirm its physical origin using multiple electrical approaches.

To further understand the adenine-WS_2 coupling effect, concentration-dependent PL measurements were performed and analyzed. Several as-prepared samples that exhibit trion-dominated emission were tested after the spin coating of adenine solutions of different concentrations. As shown in Fig. 3(a), with increasing concentration, the integrated intensities of the A^- and A components evolve oppositely. Using the same Lorentz fitting analysis discussed before, as the concentration rose from 1 μM to 2 mM, the spectral weight of the A^- component decreased, while the weight of A component increased. This excitonic evolution caused a continuous transformation of the overall PL features.

A similar trend has been reported in recent investigations of chemical doping [38]. Such quantitative control of many body states is also intrinsically correlated to the modulation of the electron density of the sample, as shown in Fig. 3(b) and concerning the band alignment (Fig. 3(c)). Theoretically, the relationship between the electron density n_e and the integrated PL intensity of A^- and A (I_{A^-} and I_A) can be modeled by a simplification of the rate equation and mass-action law (Eq. (1)) [36].

$$n_e = \frac{I_{A^-}}{I_A} \cdot \frac{\gamma_A}{\gamma_{A^-}} \cdot \frac{4m_x m_e}{\pi\hbar^2 m_{x^-}} \cdot K_b T \cdot \exp\left(-\frac{E_b}{K_b T}\right) \quad (1)$$

Here, γ_A and γ_{A^-} are the radiative decay rates of A^- and A and m_x, m_{x^-}, m_h, and m_e are the effective masses of A^-, A, holes, and electrons, respectively, where $m_{x^-} = 2m_e + m_h$ and $m_x = m_e + m_h$. In addition, $\hbar$ is the Planck's constant, K_b is the Boltzmann constant, T is the room temperature, and E_b is the binding energy of A^-. Thus, a proportional relationship for n_e and I_{A^-}/I_A is established after the careful consideration of values of other terms. Specific discussion of the approximation and choices of constant values can be found in the ESM.

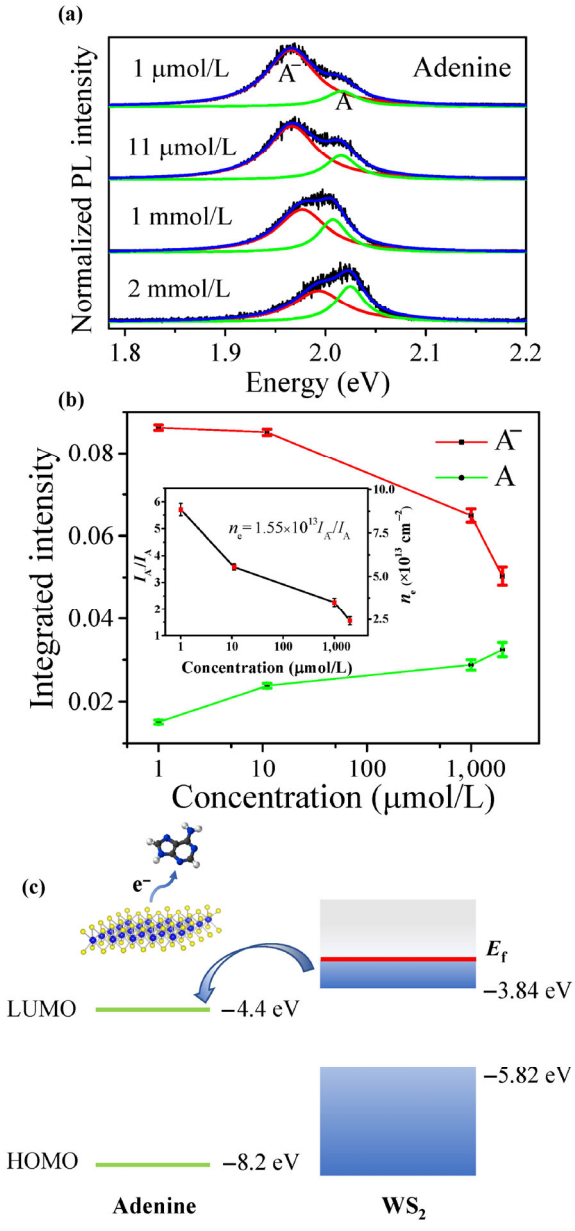

Figure 3 Further investigation of the effect of adenine on excitonic emission and electron density of WS_2. (a) PL spectra of WS_2 doped under different adenine solution concentrations, from 1 μM to 2 mM. (b) Integrated intensities of charged and neutral excitons derived from the Lorentz fitted spectra in (a). Inset shows the values of I_{A^-}/I_A and n_e under different solution concentrations with error bars. (c) The calculated electronic band structure of WS_2 and adenine, indicating the electron transfer direction.

Based on this linear relationship, using the given type of materials and experimental conditions (E_b, γ, K_b, T…), the n_e can be obtained from decomposed PL features under different adenine concentration, which yields the I_A^-/I_A values. The derived value of n_e monotonically decreased from 8.8×10^{13} to 2.4×10^{13} cm^{-2} as the solute density increased by 3 orders of magnitude. Previous investigations of the chemical doping of 1L WS_2 have reported similar n_e values [8].

This tailoring of the PL feature agrees well with the previous experimental and theoretical reports [16]. Our finding is consistent with those of a previous electrochemical investigation, which reported the electron withdrawing ability of adenine and guanine on TMDs [39]. Regarding theoretical analysis, the potential interaction mechanism between the bases and WS_2 can be understood from a microscopic point of view, considering the anchoring force, stacking configuration, and doping effects. After spin coating the nucleobase solution, the base molecules are physisorbed onto the WS_2 surface. The binding energy and distance were estimated to be around 0.2 eV and 4 Å [16, 18, 40], respectively. Based on calculations [16, 40], guanine and adenine generally have larger binding energies than cytosine and thymine, which indicate stronger interactions and agree with our PL responses. The possible geometries of the nucleobases with respect to the WS_2 basal plane have also been suggested, from parallel [40] to tilted by up to 40° [41]. The large tilting angles can be possibly attributed to concentration-induced stacking effects [8] and the presence of defect sites [9, 42] or solvent molecules [40] on the sample surfaces, which could strongly interact with the base molecules. Subsequently, an interfacial dipole between the base and WS_2 is generated, enabling the charge transfer process, which was calculated to be 0.01e per nucleobase molecule on a 5 × 5 WS_2 unit cell [16]. This doping effect was equivalently predicted by the pronounced modification of the work function/Fermi level and density of states of WS_2 [43]. The depletion of electrons is caused by charge transfer between 1L WS_2 and adenine, as schematically shown in Fig. 3(c). Considering the band alignment, Fig. 3(c) shows the computed minimum of the conduction band (–3.84 eV) and the maximum of the valence band (–5.82 eV) of 1L WS_2, as well as the highest occupied molecular orbital/lowest occupied molecular orbital (HOMO/LUMO) energies of adenine [43–45]. The as-grown sample is intrinsically n-doped, as reflected by the trion dominated PL features, which leaves the Fermi level of 1L WS_2 above the bottom of the conduction band. This band offset results in a charge transfer process from WS_2 to adenine, which neutralizes the WS_2 sample and diminishes trion formation. As the concentration of adenine coated on WS_2 increased, more electrons were extracted from the as-grown n-doped sample, resulting in the further excitonic evolution of the PL feature.

Our findings indicate that, upon the physisorption of adenine, the electron density of 1L WS_2 is strongly modulated. In addition, the spectral weight transformation from A^- to A indicates the control of the excitonic emission states of WS_2, which correlates with the dopant concentration. Such numerical correlation is beneficial as a sensing index for detecting the strength of the nucleobase solution.

Thus, the 1L CVD WS_2 platform may serve as an alternative optical sensor for nucleobases. Compared to MoS_2, our WS_2 samples yield a much stronger emission [32] and a clear peak splitting with two distinct peaks for the optical signatures of A and A^-, allowing the precise fitting of multiple peaks, which is vital for the study of the evolution of excitonic emissions. The easy coating procedure on the as-grown sample causes a significant signal change, which is equally effective but much more convenient than previously reported fluorescence labeling approaches [19, 29, 46]. Furthermore, the detection limit for adenine reaches the micromolar level. With further signal amplification, such as by applying a TMD-gold plasmonic structure [47], the limit may even reach the nanomolar or even picomolar level.

To directly observe the p-type doping effect of the adenine on 1L WS_2, a back-gated field effect transistor was fabricated and measured before and after coating with the adenine solution. Figure S2(a) in the ESM shows an optical image of the 1L WS_2 FET device which was fabricated via a standard electron-beam lithography process. We used a mechanically exfoliated monolayer sample for the devices, which show a clear transport curve profile and offer the opportunity to observe any shifts in the threshold voltage [8].

Figure S2(b) in the ESM is the corresponding fluorescence image of the 1L WS_2 device. The bright fluorescence feature indicates that the monolayer channel persists and remains an intense emission after device fabrication. In Fig. 4(a), electrical transport curves of the 1L WS_2 device with and without the 0.7 mM adenine solution coating are shown. As shown by the red curve, the typical drain-source current verus back-gate voltage (I_{ds}–V_{bg}) transport property of the as-fabricated device was measured at a bias voltage (V_{ds}) of 5 V. The result shows an unambiguous n-type behavior. After depositing adenine, as depicted by the green curve, the threshold voltage shifts toward the positive region compared to that of the bare WS_2 device. Such a shift in the threshold voltage and decreased current scale are strong evidence of a reduction in the electron density in the WS_2 sample via charge transfer induced by nucleobase adsorption on the 2D semiconductor surface. This kind of p-type doping is shown in the electrical transport characteristics and is in good agreement with our findings from the optical measurements discussed above.

To further reveal the effect of adenine on WS_2, especially on the carrier concentration when applying a gate voltage (carrier injection), gate dependent PL measurements before and after coating with the adenine solution were performed (Figs. 4(b) and 4(c)). Upon applying different gate voltages, a series of shifts in the PL profile were observed. Under each applied voltage, the evolution of the excitonic states caused by the adenine coating was well conserved. As the gate voltage increased, the spectra of the as-prepared and the doped WS_2 transformed differently, which can be attributed to the altered response to the electrical carrier injection. Consequently, an offset in PL feature, parallel to the voltage shift in the I_{ds}–V_{bg} measurement in Fig. 4(a), was discovered. For example, the PL excitonic feature of pure WS_2 under –35 V is comparable to that of adenine/WS_2 at a voltage of –25 V (Fig. S3(b) in the ESM), indicating a voltage displacement at around 10 V. Within the same framework, we applied the derived I_{A^-}/I_A value and calculated the related n_e to illustrate the p-doping effect of adenine on WS_2 (Fig. 4(d)). The n_e can be relatively well fit by a linear function for both scenarios. In the adenine/WS_2 case, the fitting residuals are nearly

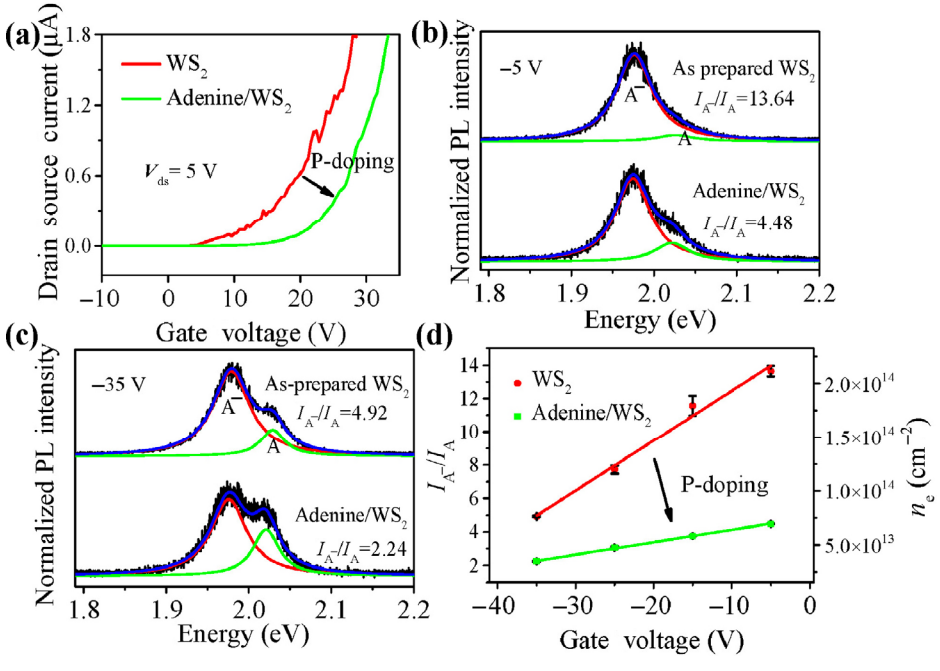

Figure 4 Modulation of transport properties and gated PL features of exfoliated 1L WS_2 with a coating of adenine. (a) I_{ds}–V_{bg} curves at V_{ds} = 5 V for the as-fabricated device and the device with the coating of 0.7 mM adenine solution. (b) and (c) The Lorentz-fitted PL spectra of the as-prepared 1L WS_2 and WS_2 coated with 0.34 mM adenine solution at gate voltages of –35 and –5 V. (d) The intensity ratio between trion and neutral exciton (I_{A^-}/I_A) and the electron concentration (n_e) of the WS_2 with/without coating as a function of gate voltage. The straight lines are the linear fits for I_{A^-}/I_A and n_e with error bars.

negligible. This proves that our preferred theoretical framework to determine n_e is reasonable, considering the linear carrier-injecting nature of gate doping [6]. The difference in the slope of n_e–V_{bg} indicates a four-fold suppression of carrier injection because of the p-type doping from adenine. These observations reflect the reduction in the electron concentration of the sample. In addition, we fabricated few-layer WS_2 (Fig. S4 in the ESM) and MoS_2 (Fig. S1(b) in the ESM) devices and observed a similar doping effect in the electrical measurement, indicating the general electron affinity of adenine when attached to layered TMDs.

This kind of p-type doping is expected to be a universal effect for other 1L TMD materials like MoS_2 (Fig. S1 in the ESM). Besides, because the optical response of guanine on our CVD WS_2 platform has also been observed, based on a comparison of the same solution concentrations shown in Figs. 2(b) and 2(c), adenine and guanine exhibit different effects on the PL profile and can be quantitatively distinguished based on their different PL evolution trends. The PL profile shows the different responses for adenine and guanine and the calculated I_{A^-}/I_A is 6.930 for guanine and 2.256 for adenine, which indicates a disparity in the electron modulation ability of these two dopants. Previous theoretical works have reported less pronounced shifts in the density states of the WS_2–nucleobase complexes of cytosine and thymine, indicating their generally less effective reduction of the electron density in the WS_2 sample [16]. In this work, we observed a negligible impact of cytosine and thymine on WS_2. This is possibly due to the difference in electron withdrawing ability relative to n-type WS_2 between adenine, guanine, cytosine, and thymine. The overall three kinds of optical responses on our WS_2 platform in the four cases demonstrate an acceptable selectivity for sensing nucleobases. To further distinguish cytosine and thymine, more strategies and systems must be explored.

3 Conclusions

Through experiments, we found that WS_2 monolayers exhibit a tunable optical excitonic emission after coating by nucleobases. This phenomenon was further investigated and explained as the result of the charge transfer process generated between the bases and WS_2. Our hypothesis is proven by PL spectra and further supported by the electrical transport measurements. In a typical example, a simple and effective modulation of the excitonic features of monolayer WS_2 was demonstrated via the physisorption of adenine, which should also be applicable to other bases such as guanine and other TMD materials. We believe this is a cornerstone study for the development of future optical sensing, illustrating an alternative way to use TMD materials in biological applications.

4 Methods

4.1 Materials

All DNA nucleobases powders were purchased from Sigma-Aldrich (Singapore). The powders were dissolved in conventional organic solvents (ethanol and isopropyl alcohol) and water and sonicated for 30 min to obtain clear solutions with micro- to millimolar concentrations. The as-prepared solutions and solvents for the control experiment were spin coated onto the wafer at 1,000 rpm for 60 s to avoid leaving residues because of the liquid–substrate affinity.

4.2 Preparation of WS_2 samples

The CVD WS_2 flakes were directly grown on standard 300-nm SiO_2/Si wafer substrates via the sulfurization of WO_3 powders, as reported previously [31, 32]. As for the exfoliated samples, they were produced by mechanical exfoliation from commercial bulk WS_2 crystals purchased from 2D Semiconductors Inc., also onto highly doped 300 nm SiO_2/Si wafer.

4.3 Device fabrication

A 5-nm layer of Cr and an 80-nm layer of Au as source and drain electrodes, respectively, were deposited by thermal evaporation after using a standard electron-beam lithography process to pattern the contact electrodes, followed by a lift off process in acetone to obtain well-defined metal electrodes. All electrical transport measurements were conducted under vacuum (~10^{-5} mbar) at room temperature using an Agilent

Technologies B1500A semiconductor device analyzer.

4.4 Optical characterization

The micro-PL and Raman measurements were performed with a WITec CRM 200 system. We used an excitation laser with a wavelength of 532 nm for the PL and Raman measurements. The laser power was kept lower than 60 μW to avoid heating effects. The gate-dependent PL measurement was conducted using the same WITec system with the substrate loaded into the Linkam stage and connected with a Keithley 4200-SCS semiconductor characterization system. The configuration remained the same before and after the solution was spin coated.

Acknowledgements

This work is supported by the Singapore Ministry of Education under MOE Tier 1 RG178/15 and MOE Tier 1 RG100/15. C. X. C. thanks the support by the National Young 1000 Talent Plan of China and the Shanghai Municipal Natural Science Foundation (No. 16ZR1402500). M. E. appreciates the support by National Synergetic Innovation Center for Advanced Materials (SICAM), the start-up fund by Nanjing Tech University, and Jiangsu 100 Talent.

Electronic Supplementary Material: Supplementary material (calculation of electron density via PL spectrum of monolayer WS_2, optical and electrical characterization of MoS_2 coated with adenine, electrical response for few layer WS_2 device and Raman mapping characterization before and after coating) is available in the online version of this article at https://doi.org/10.1007/s12274-017-1792-z.

References

[1] Berghäuser, G.; Malic, E. Analytical approach to excitonic properties of MoS_2. *Phys. Rev. B* **2014**, *89*, 125309.

[2] Ramasubramaniam, A. Large excitonic effects in monolayers of molybdenum and tungsten dichalcogenides. *Phys. Rev. B* **2012**, *86*, 115409.

[3] Wang, Q. H.; Kalantar-Zadeh, K.; Kis, A.; Coleman, J. N.; Strano, M. S. Electronics and optoelectronics of two-dimensional transition metal dichalcogenides. *Nat. Nanotechnol.* **2012**, *7*, 699–712.

[4] Mak, K. F.; Lee, C.; Hone, J.; Shan, J.; Heinz, T. F. Atomically thin MoS_2: A new direct-gap semiconductor. *Phys. Rev. Lett.* **2010**, *105*, 136805.

[5] Huard, V.; Cox, R. T.; Saminadayar, K.; Arnoult, A.; Tatarenko, S. Bound states in optical absorption of semiconductor quantum wells containing a two-dimensional electron gas. *Phys. Rev. Lett.* **2000**, *84*, 187–190.

[6] Mak, K. F.; He, K. L.; Lee, C. G.; Lee, G. H.; Hone, J.; Heinz, T. F.; Shan, J. Tightly bound trions in monolayer MoS_2. *Nat. Mater.* **2013**, *12*, 207–211.

[7] Shang, J. Z.; Shen, X. N.; Cong, C. X.; Peimyoo, N.; Cao, B. C.; Eginligil, M.; Yu, T. Observation of excitonic fine structure in a 2D transition-metal dichalcogenide semiconductor. *ACS Nano* **2015**, *9*, 647–655.

[8] Peimyoo, N.; Yang, W. H.; Shang, J. Z.; Shen, X. N.; Wang, Y. L.; Yu, T. Chemically driven tunable light emission of charged and neutral excitons in monolayer WS_2. *ACS Nano* **2014**, *8*, 11320–11329.

[9] Nan, H. Y.; Wang, Z. L.; Wang, W. H.; Liang, Z.; Lu, Y.; Chen, Q.; He, D. W.; Tan, P. H.; Miao, F.; Wang, X. R. et al. Strong photoluminescence enhancement of MoS_2 through defect engineering and oxygen bonding. *ACS Nano* **2014**, *8*, 5738–5745.

[10] Wang, Y. L.; Cong, C. X.; Yang, W. H.; Shang, J. Z.; Peimyoo, N.; Chen, Y.; Kang, J. Y.; Wang, J. P.; Huang, W.; Yu, T. Strain-induced direct–indirect bandgap transition and phonon modulation in monolayer WS_2. *Nano Res.* **2015**, *8*, 2562–2572.

[11] Kim, E.; Ko, C.; Kim, K.; Chen, Y. B.; Suh, J.; Ryu, S.-G.; Wu, K. D.; Meng, X. Q.; Suslu, A.; Tongay, S. et al. Site selective doping of ultrathin metal dichalcogenides by laser-assisted reaction. *Adv. Mater.* **2016**, *28*, 341–346.

[12] Amani, M.; Lien, D.-H.; Kiriya, D.; Xiao, J.; Azcatl, A.; Noh, J.; Madhvapathy, S. R.; Addou, R.; KC, S.; Dubey, M. et al. Near-unity photoluminescence quantum yield in MoS_2. *Science* **2015**, *350*, 1065–1068.

[13] Han, H. V.; Lu, A. Y.; Lu, L. S.; Huang, J. K.; Li, H. N.; Hsu, C. L.; Lin, Y. C.; Chiu, M. H.; Suenaga, K.; Chu, C. W. et al. Photoluminescence enhancement and structure repairing of monolayer $MoSe_2$ by hydrohalic acid treatment. *ACS Nano* **2016**, *10*, 1454–1461.

[14] Tongay, S.; Zhou, J.; Ataca, C.; Liu, J.; Kang, J. S.; Matthews, T. S.; You, L.; Li, J. B.; Grossman, J. C.; Wu, J. Q. Broad-range modulation of light emission in two-dimensional semiconductors by molecular physisorption gating. *Nano Lett.* **2013**, *13*, 2831–2836.

[15] Mouri, S.; Miyauchi, Y.; Matsuda, K. Tunable photoluminescence of monolayer MoS_2 via chemical doping. *Nano Lett.* **2013**, *13*, 5944–5948.

[16] Vovusha, H.; Sanyal, B. Adsorption of nucleobases on 2D transition-metal dichalcogenides and graphene sheet: A first principles density functional theory study. *RSC Adv.* **2015**, *5*, 67427–67434.

[17] Farimani, A. B.; Min, K.; Aluru, N. R. DNA base detection using a single-layer MoS_2. *ACS Nano* **2014**, *8*, 7914–7922.

[18] Sharma, M.; Kumar, A.; Ahluwalia, P. K. Optical fingerprints and electron transport properties of DNA bases adsorbed on monolayer MoS_2. *RSC Adv.* **2016**, *6*, 60223–60230.

[19] Zhang, Y.; Zheng, B.; Zhu, C. F.; Zhang, X.; Tan, C. L.; Li, H.; Chen, B.; Yang, J.; Chen, J. Z.; Huang, Y. et al. Single-layer transition metal dichalcogenide nanosheet-based nanosensors for rapid, sensitive, and multiplexed detection of DNA. *Adv. Mater.* **2015**, *27*, 935–939.

[20] Chen, J.; Gao, C. J.; Mallik, A. K.; Qiu, H. D. A WS_2 nanosheet-based nanosensor for the ultrasensitive detection of small molecule–protein interaction via terminal protection of small molecule-linked DNA and Nt.BstNBI-assisted recycling amplification. *J. Mater. Chem. B* **2016**, *4*, 5161–5166.

[21] Zhao, J. J.; Jin, X.; Vdovenko, M.; Zhang, L. L.; Sakharov, I. Y.; Zhao, S. L. A WS_2 nanosheet based chemiluminescence resonance energy transfer platform for sensing biomolecules. *Chem. Commun.* **2015**, *51*, 11092–11095.

[22] Macwan, I.; Khan, M. D. H.; Aphale, A.; Singh, S.; Liu, J.; Hingorani, M.; Patra, P. Interactions between avidin and graphene for development of a biosensing platform. *Biosens. Bioelectron.* **2017**, *89*, 326–333.

[23] Loan, P. T. K.; Zhang, W. J.; Lin, C. T.; Wei, K. H.; Li, L. J.; Chen, C. H. Graphene/MoS_2 heterostructures for ultrasensitive detection of DNA hybridisation. *Adv. Mater.* **2014**, *26*, 4838–4844.

[24] Ananthanarayanan, A.; Wang, X. W.; Routh, P.; Sana, B.; Lim, S.; Kim, D. H.; Lim, K. H.; Li, J.; Chen, P. Facile synthesis of graphene quantum dots from 3D graphene and their application for Fe^{3+} sensing. *Adv. Funct. Mater.* **2014**, *24*, 3021–3026.

[25] Ananthanarayanan, A.; Wang, Y.; Routh, P.; Sk, M. A.; Than, A.; Lin, M.; Zhang, J.; Chen, J.; Sun, H. D.; Chen, P. Nitrogen and phosphorus co-doped graphene quantum dots: Synthesis from adenosine triphosphate, optical properties, and cellular imaging. *Nanoscale* **2015**, *7*, 8159–8165.

[26] Zeng, S. W.; Sreekanth, K. V.; Shang, J. Z.; Yu, T.; Chen, C. K.; Yin, F.; Baillargeat, D.; Coquet, P.; Ho, H. P.; Kabashin, A. V. et al. Graphene–gold metasurface architectures for ultrasensitive plasmonic biosensing. *Adv. Mater.* **2015**, *27*, 6163–6169.

[27] Li, Z.; Chen, Y.; Li, X.; Kamins, T.; Nauka, K.; Williams, R. S. Sequence-specific label-free DNA sensors based on silicon nanowires. *Nano Lett.* **2004**, *4*, 245–247.

[28] Star, A.; Tu, E.; Niemann, J.; Gabriel, J.-C. P.; Joiner, C. S.; Valcke, C. Label-free detection of DNA hybridization using carbon nanotube network field-effect transistors. *Proc. Natl. Acad. Sci. USA* **2006**, *103*, 921–926.

[29] Zhu, C. F.; Zeng, Z. Y.; Li, H.; Li, F.; Fan, C. H.; Zhang, H. Single-layer MoS_2-based nanoprobes for homogeneous detection of biomolecules. *J. Am. Chem. Soc.* **2013**, *135*, 5998–6001.

[30] Lee, J.; Dak, P.; Lee, Y.; Park, H.; Choi, W.; Alam, M. A.; Kim, S. Two-dimensional layered MoS_2 biosensors enable highly sensitive detection of biomolecules. *Sci. Rep.* **2014**, *4*, 7352.

[31] Beaudet, A. L.; Belmont, J. W. Array-based DNA diagnostics: Let the revolution begin. *Annu. Rev. Med.* **2008**, *59*, 113–129.

[32] Peimyoo, N.; Shang, J. Z.; Cong, C. X.; Shen, X. N.; Wu, X. Y.; Yeow, E. K. L.; Yu, T. Nonblinking, intense two-dimensional light emitter: Monolayer WS_2 triangles. *ACS Nano* **2013**, *7*, 10985–10994.

[33] Cong, C. X.; Shang, J. Z.; Wu, X.; Cao, B. C.; Peimyoo, N.; Qiu, C. Y.; Sun, L. T.; Yu, T. Synthesis and optical properties of large-area single-crystalline 2D semiconductor WS_2 monolayer from chemical vapor deposition. *Adv. Opt. Mater.* **2014**, *2*, 131–136.

[34] Berkdemir, A.; Gutiérrez, H. R.; Botello-Méndez, A. R.; Perea-López, N.; Elías, A. L.; Chia, C.-I.; Wang, B.; Crespi, V. H.; López-Urías, F.; Charlier, J.-C. et al. Identification of individual and few layers of WS_2 using Raman spectroscopy. *Sci. Rep.* **2013**, *3*, 1755.

[35] Zeng, H. L.; Liu, G.-B.; Dai, J. F.; Yan, Y. J.; Zhu, B. R.; He, R. C.; Xie, L.; Xu, S. J.; Chen, X. H.; Yao, W. et al. Optical signature of symmetry variations and spin-valley coupling in atomically thin tungsten dichalcogenides. *Sci. Rep.* **2013**, *3*, 1608.

[36] Gutiérrez, H. R.; Perea-López, N.; Elías, A. L.; Berkdemir, A.; Wang, B.; Lv, R. T.; López-Urías, F.; Crespi, V. H.; Terrones, H.; Terrones, M. Extraordinary room-temperature photoluminescence in triangular WS_2 monolayers. *Nano Lett.* **2013**, *13*, 3447–3454.

[37] Ross, J. S.; Wu, S. F.; Yu, H. Y.; Ghimire, N. J.; Jones, A. M.; Aivazian, G.; Yan, J. Q.; Mandrus, D. G.; Xiao, D.; Yao, W. et al. Electrical control of neutral and charged excitons in a monolayer semiconductor. *Nat. Commun.* **2013**, *4*, 1474.

[38] Ryder, C. R.; Wood, J. D.; Wells, S. A.; Hersam, M. C. Chemically tailoring semiconducting two-dimensional transition metal dichalcogenides and black phosphorus. *ACS Nano* **2016**, *10*, 3900–3917.

[39] Cho, B.; Yoon, J.; Lim, S. K.; Kim, A. R.; Kim, D.-H.; Park, S.-G.; Kwon, J.-D.; Lee, Y.-J.; Lee, K.-H.; Lee, B. H. et al.

Chemical sensing of 2D graphene/MoS_2 heterostructure device. *ACS Appl. Mater. Interfaces* **2015**, *7*, 16775–16780.

[40] Liang, L. J.; Hu, W.; Xue, Z. Y.; Shen, J.-W. Theoretical study on the interaction of nucleotides on two-dimensional atomically thin graphene and molybdenum disulfide. *FlatChem* **2017**, *2*, 8–14.

[41] Dontschuk, N.; Stacey, A.; Tadich, A.; Rietwyk, K. J.; Schenk, A.; Edmonds, M. T.; Shimoni, O.; Pakes, C. I.; Prawer, S.; Cervenka, J. A graphene field-effect transistor as a molecule-specific probe of DNA nucleobases. *Nat. Commun.* **2015**, *6*, 6563.

[42] Zhou, W.; Zou, X. L.; Najmaei, S.; Liu, Z.; Shi, Y. M.; Kong, J.; Lou, J.; Ajayan, P. M.; Yakobson, B. I.; Idrobo, J.-C. Intrinsic structural defects in monolayer molybdenum disulfide. *Nano Lett.* **2013**, *13*, 2615–2622.

[43] Lee, J.-H.; Choi, Y.-K.; Kim, H.-J.; Scheicher, R. H.; Cho, J.-H. Physisorption of DNA nucleobases on h-BN and graphene: vdW-corrected DFT calculations. *J. Phys. Chem. C* **2013**, *117*, 13435–13441.

[44] Hawke, L. G. D.; Kalosakas, G.; Simserides, C. Electronic parameters for charge transfer along DNA. *Eur. Phys. J. E* **2010**, *32*, 291.

[45] Kang, J.; Tongay, S.; Zhou, J.; Li, J. B.; Wu, J. Q. Band offsets and heterostructures of two-dimensional semiconductors. *Appl. Phys. Lett.* **2013**, *102*, 012111.

[46] Xi, Q.; Zhou, D.-M.; Kan, Y.-Y.; Ge, J.; Wu, Z.-K.; Yu, R.-Q.; Jiang, J.-H. Highly sensitive and selective strategy for microRNA detection based on WS_2 nanosheet mediated fluorescence quenching and duplex-specific nuclease signal amplification. *Anal. Chem.* **2014**, *86*, 1361–1365.

[47] Wang, Z.; Dong, Z. G.; Gu, Y. H.; Chang, Y.-H.; Zhang, L.; Li, L.-J.; Zhao, W. J.; Eda, G.; Zhang, W. J.; Grinblat, G. et al. Giant photoluminescence enhancement in tungsten-diselenide–gold plasmonic hybrid structures. *Nat. Commun.* **2016**, *7*, 11283.